ECCOMAS Congress 2016
VII European Congress on Computational Methods in Applied Sciences and Engineering
M. Papadrakakis, V. Papadopoulos, G. Stefanou, V. Plevris (eds.)
Crete Island, Greece, 5–10 June 2016

PERFORMANCE IMPROVEMENT OF FLOW COMPUTATIONS WITH AN OVERSET-GRID METHOD INCLUDING BODY MOTIONS USING A FULL MULTIGRID METHOD

Kunihide Ohashi[1], **Hiroshi Kobayashi**[2]

[1]National Maritime Research Institute
6-38-1 Shinkawa Mitaka Tokyo Japan
e-mail: k-ohashi@nmri.go.jp

[2]National Maritime Research Institute
6-38-1 Shinkawa Mitaka Tokyo Japan
e-mail: hiroshi@nmri.go.jp

Keywords: Overset-Grid Method, Full Multigrid Method, 3D RANS, Free Surface

Abstract. *A full multigrid method with an overset-grid method is developed to get a fast convergence. The weight values for an overstet-grid interpolation of flow variables can be determined on the fine grid level of multigrid, however, the weight value might be difficult to determine on coarser grid level. Therefore, the receptor cell value on coarser grid level is set and kept by the interpolation and correction of the multigrid method. Then, the flow variables on the coarse grid is interpolated to the fine grid as initial flows of the full multigrid method. The present method is applied to steady and unsteady simulations. The elapased time of steady simulations with and without free surafce is reduced about 35% of the time without the full multigrid method. The present method also succeeds to reduce the computational time remarkably on the unsteady simulation.*

1 INTRODUCTION

An overset-grid method can treat complex geometries by assembling the computational grid around each geometry and generating the overset information to combine the all grids. Additionally, the overset-grid method has a lot of flexibility in design processes, various appended shapes can be computed without generating the all computational grid just by replacing the computational grid around an appendage and generating the overset information.

The overset relation is generally composed on the certain division number of grid points, and performance improvement method to reduce a computational time plays important role with increasing the number of grid points.

The full multigrid method(FMG) is efficient to get fast convergence. A flow computation is started from the coarsest grid on the multigrid level, then the flow variables are interpolated to the finer grid as the initial flow. The interpolation cycle is continued until the finest grid level. The weight values for the overset-grid interpolation of flow variables can be determined on the finest grid of multigrid level, however, the weight value might be difficult to determine on coarser grid level. Therefore, the flow variables of the coarse grid are interpolated to the finest grid, then values are updated by using the overset interpolation on the finest grid. After the interpolation, the flow variables on the finest grid level are transformed to the coarser grid level and maintained the values. The computation on the coarse grid level is continued with using the overset interpolated values. Then, the flow variables on the coarse grid are interpolated to finer grid level as the initial flow of the full multigrid method.

The present method is applied to steady simulations w/ and w/o a free surface with several appendages to a ship hull. Then, the method is applied to an unsteady simulation including a body motion. Through the comparisons of results with and without FMG, the effectiveness of the present method is examined.

2 COMPUTATIONAL METHOD

2.1 Base solver

An in-house structured CFD solver[1] is employed. The governing equation is 3D RANS equation for incompressible flows. Artificial compressibility approach is used for the velocity-pressure coupling. Spatial discretization is based on a finite-volume method. A cell centered layout is adopted in which flow variables are defined at the centroid of each cell and a control volume is a cell itself. Inviscid fluxes are evaluated by the third-order upwind scheme based on the flux-difference splitting of Roe. The evaluation of viscous fluxes is second-order accurate. For unsteady flow simulations, a dual time stepping approach is used in order to recover incompressibility at each time step. It is consisted from the second order two-step backward scheme for the physical time stepping and the first order Euler implicit scheme for the pseudo time. The linear equation system is solved by the symmetric Gauss-Seidel (SGS) method.

For free surface treatment, an interface capturing method with a single phase level set approach is employed.

Body motions are taken into account by a moving grid technique. Grid velocities are contained in the inviscid terms to satisfy the geometrical conservation law. The grid velocities are derived from the volume where an each cell face sweeps. The boundary condition on a body is given as the velocities of the body motion.

2.2 Overset-grid method

The weight values for the overset-grid interpolation are determined by an in-house system[2]. The detail of the system can be found on [2], the summary is described.

1. The priority of the computational grid is set.
2. The cells of a lower priority grid and inside a body is identified (called as in-wall cell in here).
3. Receptors cells which the flow variables have to be interpolated from donor cells are defined. Two cells on a higher priority grid and facing to the outer boundary are set as receptor cells to satisfy the third order discretization of NS solver. Additionally, two cells neighborhood of in-wall cells, the cells of a lower priority grid and inside the domain of a higher priority grid are also set as the receptor cell.
4. The weight values for the overset interpolation are determined by solving the inverse problem based on Ferguson spline interpolation.

Flow variables of the receptor cell are updated when the boundary condition is set. The forces and moments are integrated on the higher priority grid to eliminate the lapped region on body surfaces. At first, the cell face of the lower priority grid is divided into small pieces. Secondly, the small piece is projected to the cell face of the higher priority grid by using the normal vector of the higher priority face. Then the 2D solid angle is computed and the small piece is decided in or out of the higher priority face. Once the small piece is in the higher priority face, the area ratio of the piece is set to zero. Finally, the area ratio is integrated on the lower priority face, then we have the ratio to integrate the forces and moments on lower priority face.

2.3 Full multigrid method

The multigrid method can obtain a fast convergence by reducing the residual which has the large wave length on a coarse grid. The agglomerate type is applied to the present method. A coarse grid is defined two cells in each (i, j, k) direction, thus one cell on the coarse grid is constructed by eight cells on the fine grid.

The solution $\boldsymbol{q}_l$ on the fine grid level(l) is transferred to the coarse grid level($l+1$) as follows.

$$\boldsymbol{q}_{l+1} = T^l_{l+1}\boldsymbol{q}_l \tag{1}$$

where T^l_{l+1} is defined as

$$T^l_{l+1}\boldsymbol{q}_l = (\Sigma \boldsymbol{q}_l V_l)/V_{l+1} \tag{2}$$

The equation to be solved on the coarse grid level is expressed as

$$\frac{\partial \boldsymbol{q}_{l+1} V_{l+1}}{\partial \tau} = -\boldsymbol{R}_{l+1}(\boldsymbol{q}_{l+1}) - \boldsymbol{P}_{l+1} \tag{3}$$

where $\boldsymbol{R_{l+1}}$ is the residual on the coarse grid, and the forcing term $\boldsymbol{P}_{l+1}$ is given as follows.

$$\boldsymbol{P}_{l+1} = Q^{l+1}_l \boldsymbol{R}_l(\boldsymbol{q}_l) - \boldsymbol{R}_{l+1}(\boldsymbol{q}_{l+1}) \tag{4}$$

where Q_l^{l+1} is transfer operator for the residual and is defined by the sum of eight cells on the fine grid.

$$Q_l^{l+1}\boldsymbol{R}_l(\boldsymbol{q}_l) = \Sigma(\boldsymbol{R}_l) \tag{5}$$

The solution on the coarse grid is expressed as $\boldsymbol{q}_{l+1}^+$, then the correction to the fine grid level is defined as

$$\boldsymbol{q}_l^+ = \boldsymbol{q}_l + I_{l+1}^l(\boldsymbol{q}_{l+1}^+ - \boldsymbol{q}_{l+1}) \tag{6}$$

where I_{l+1}^l is an interpolation operator for a correction.

The computation starts from the coarsest grid on FMG, then the the solution is interpolated to the finer grid as the initial flows, and FMG achieves the fast convergence. An overset relation can be determined on the finest grid, however the relation may be difficult to construct on a coarse grid level. An additional method is required to apply FMG for the overset-grid. While one solving the equation on a coarse grid level, the solution interpolation and transfer of multi-grid method are made in a specific computational step. The receptor cell value is updated on the finest grid level, then transferred to coarser grid level. The present method can take account the receptor value on coarser grid level. The influence of a specific computational step(SCS) is also investigated in the present research.

The cell flag to be solved or unsolved on a coarse grid level is determined by using the cell flag on a fine grid level. An unsolved cell flag is included in the cell on a coarse grid, the cell is flagged as an unsolved cell(Fig.1). And furthermore, a cell flag on the coarser grid level is determined in the same way. Once the receptor cell value on the finest grid is included in coarser grid level, the correction to the finer grid from a coarse grid is treated as zero.

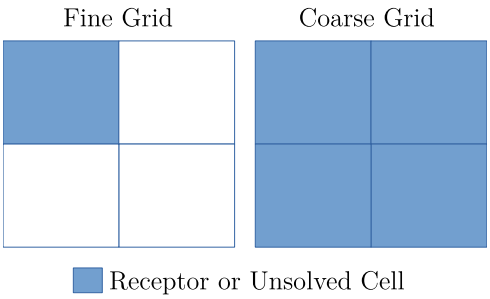

Figure 1: Flagging of cells with multigrid level

3 COMPUTED RESULTS

3.1 Steady double model flow

The FMG and overset-grid methods are applied to the flows around a main hull with several appendages. Reynolds number is 3.0×10^6 and EASM[3] is applied to compute Reynolds stresses. Table 1 shows the division number of computational grids in each direction. The grids are arranged with the priority of the overset interpolation. As appendages, two bilge keels, two aft hull fins, one duct which is situated just before a propeller, and a rudder are arranged with refined rectangular grids which resolve the flows around the aft fins and the rudder. The computational grid are consisted from 10 grids with about 3.0 millions cells.

Table 1: Division number of computational grid

Grid	IM×JM×KM
Bilge keel×2	33×65×57
Aft fin×2	49×65×41
Rect. fin1,2	53×33×65
Duct	61×61×37
Rudder	101×81×73
Rect.	101×81×73
Hull	113×121×77

Table 2: Number of solved cell

Grid	Fine		Medium		Coarse	
	total	solved	total	solved	total	solved
Bilge keel×2	229376	69632	28672	8704	3584	896
Aft fin×2	245760	116736	30720	14592	3840	1536
Rect. fin1	212992	65901	26624	7878	3328	1
Rect. fin2	212992	66044	26624	7889	3328	0
Duct	129600	124936	16200	15436	2025	1440
Rudder	576000	297152	72000	36996	9000	3894
Rect.	576000	269380	72000	31412	9000	242
Hull	1021440	908720	127680	111726	15960	11526

Three levels multigrid method is applied. Table 2 shows the total and solved cell number with the multigrid level. The cell number to be solved becomes zero on the refined rectangular grid at the coarse grid level, hence the full multigrid starts with the medium grid.

Fig.2 shows the time history of L2-norm of the pressure with changing the SCS from 5 to 40. Fig.3, 4 show the comparisons of the total resistance coefficient and the elapsed time. The total resistance coefficient is non-dimensionalized by $\frac{1}{2}\rho U_0^2 L_0^2$. The spikes of L2-norm are existed when the interpolation and the correction of the multigrid are made with SCS intervals. The difference of L2-norm between SCS=5 and 10 is small, while L2-norm becomes larger after 301 time steps where the computational grid changes to the fine grid with using SCS=20 and 40. The total resistance coefficient shows small difference with the SCS change until 300 time steps, while larger fluctuation with SCS=20 and 40 appears after 301 time steps. From the above results, SCS is determined as 10 from hereafter.

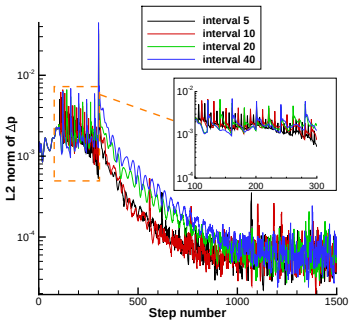

Figure 2: Time history of L2 norm(Δp)

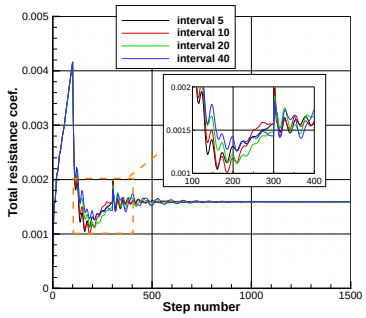

Figure 3: Convergence history of total resistance coefficient

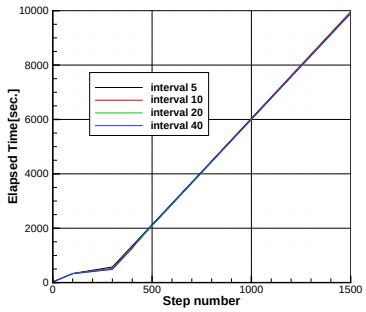

Figure 4: Comparison of elapsed time

From Fig.5 to Fig.7 show the comparisons of the results with and without FMG. The time history of L2-norm of FMG has the spike on 301 time steps when the computational grid shifts from the medium level to the fine level(Fig.5). FMG takes few times until 300 time steps with the computation on the medium grid, then the slope of FMG becomes same as the result without FMG(Fig.7). The steps from 500 to 800 where the total resistance coefficient almost converges are magnified in Fig.6, and the elapsed time at 650 steps where the total resistance coefficient converges within $\pm 0.5\%$ from the averaged value is compared. FMG takes 3271 seconds, while the multigrid(without FMG) takes 5118 seconds, thus FMG succeeds to reduce the computational time about 37% in this case.

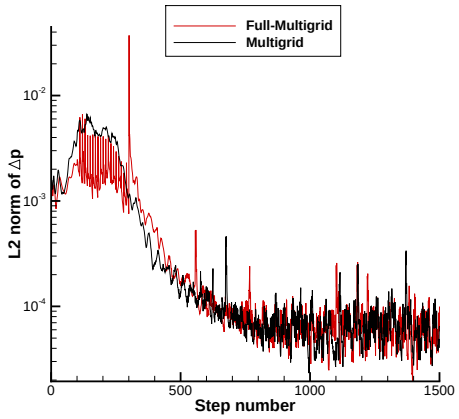

Figure 5: Comparison of L2 norm(Δp)

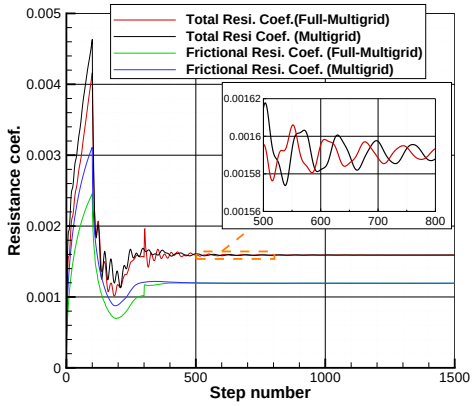

Figure 6: Convergence history of resistance coefficient

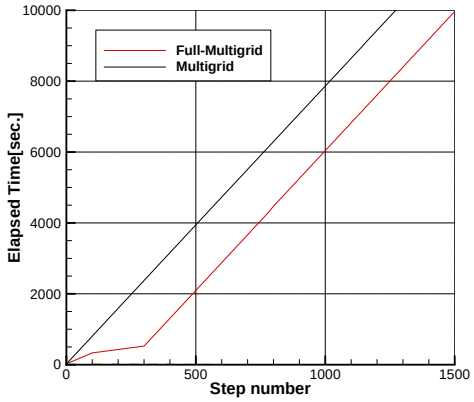

Figure 7: Comparison of elapsed time

3.2 Steady free surface flow

The FMG method is applied to the free surface flow with the overset-grid. The computational grid is consisted from 5.07 million cells with the hull grid, the rudder grid and two rectangular grids. Reynolds number is 1.074×10^7, Froude number is 0.261 and $k - \omega SST$[4] model is applied. Table 3 shows the division number of computational grids in each direction.

Table 3: Division number of computational grid

Grid	IM×JM×KM
Rudder	113×121×77
Rect. Rud.	49 × 49 × 45
Hull	113×121×77
Rect.	113×121×77

Table 4 shows the total and solved cell number with the multigrid level. The cell number to be solved remains on the coarse grid level, hence FMG starts from the coarse grid level in this case. The computation on the coarse grid level continues until 500 steps, then the computation

Table 4: Number of solved cell

Grid	Fine		Medium		Coarse	
	total	solved	total	solved	total	solved
Rudder	135168	126710	16896	15836	2112	1584
Rect. Rud.	101376	70660	12672	8606	1584	116
Hull	3276800	3149958	409600	392792	51200	43944
Rect.	1554432	1329118	194304	164464	24288	18160

continues on the medium grid, finally the computation on the fine grid level starts from 1001 steps.

Fig.8 shows the comparison of L2-norm with and without FMG. The time history of L2-norm of FMG has the spikes at 501 and 1001 time steps when the computational grid shifts from the coarse and medium grid levels to finer grid level. The total resistance coefficient also shows small diffraction when the grid level moves to finer grid level(Fig.9), then converges rapidly. The elapsed time of FMG is relatively small until the grid level reaches the fine grid, then the slope becomes same as the result without FMG(Fig.10). The steps from 1600 to 2300 where the total resistance coefficient almost converges are magnified in Fig.9. The elapsed time at 2200 steps with FMG where the total resistance coefficient converges is compared with the elapsed time without FMG at 1800 steps. FMG takes 34142 seconds, while the multigrid(without FMG) takes 52624 seconds, thus FMG succeeds to reduce the computational time about 35%.

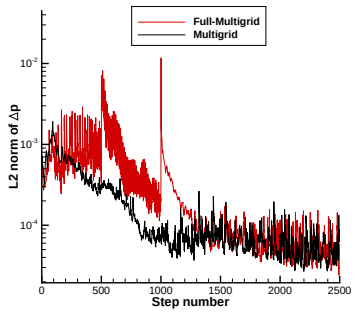

Figure 8: Comparison of L2 norm(Δp)

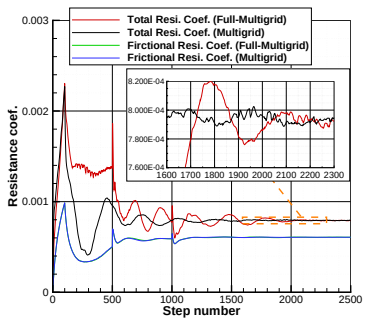

Figure 9: Convergence history of total resistance coefficient

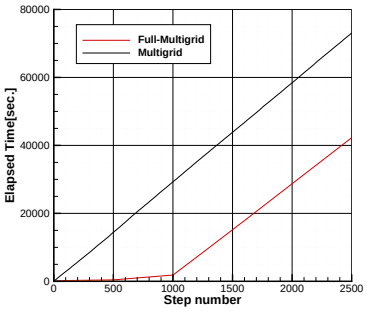

Figure 10: Comparison of elapsed time

3.3 Unsteady simulation with body motion

The FMG method is applied to the unsteady flow computation with a prescribed rotational motion. The computation of a marine propeller with a fixed revolution number is selected. All grids rotate around the x-axis with the revolution number. Reynolds number is 4.649×10^5 and $k - \omega SST$[4] model is applied. The non-dimensional revolution number is 2.0. Table 5 shows the division number of computational grids in each direction. The computational grid is consisted from 2.09 million cells with the the five blade grids and the cylinder grid on the background.

Table 5: Division number of computational grid

Grid	IM×JM×KM
Blade	49×65×33
Cylinder	117×145×97

Table 6 shows the total and solved cell number with the multigrid level. The cell number to be solved remains on the coarse grid level, hence FMG starts from the coarse grid level. The computation on the coarse grid level continues until 500 steps, then the computation continues on the medium grid level, finally the computation on the fine grid level starts from 1001 steps.

Fig.11 shows the comparison of L2-norm with and without FMG. The non-dimensionalized physical time step with FMG is 3.0×10^{-4}, while the time step without FMG is 5.0×10^{-5}, thus the time step with FMG takes larger on the present unsteady simulation. L2-norm with FMG is slightly reduced with the computational steps, while the gradient of L2-norm without FMG is comparatively small. The resistance coefficient with FMG converges rapidly, on the other hand, the resistance coefficient without FMG remains the fluctuation(Fig.12). Fig.13 shows the comparison of the elapsed time with and without FMG. Due to the difference of the physical time step, the direct comparison is difficult but the elapsed time with FMG is remarkably reduced.

Fig.14 shows the pressure distribution on the body surfaces and the velocity distribution with vectors just behind the blades. The back side of the blade surfaces becomes negative pressure values due to the angle of attack which is caused by the inflow to the blades. The axial velocity is accelerated by the blades, hence the variables are smoothly interpolated and computed in each computational grid. Thus it can be said the present overset grid-method and FMG work well.

Table 6: Number of solved cell

Grid	Fine		Medium		Coarse	
	total	solved	total	solved	total	solved
Blade1	98304	92160	12288	11520	1536	1152
Blade2	98304	92160	12288	11520	1536	1152
Blade3	98304	92160	12288	11520	1536	1152
Blade4	98304	92160	12288	11520	1536	1152
Blade5	98304	92160	12288	11520	1536	1152
Cylinder	1603584	1422870	200448	174881	25056	18866

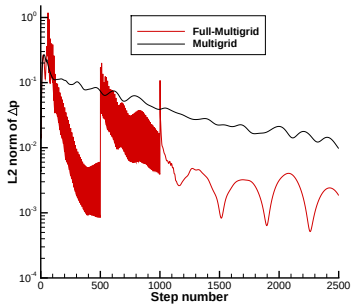

Figure 11: Comparison of L2 norm(Δp)

4 CONCLUSIONS

- The full multigrid method to the overset-grid method has been developed.
- Present method succeeds to reduce the computational time about 35% in the steady computations with and without the free surface.
- Present method also can be applied to the unsteady simulation, and the elapsed time of the computation is remarkably reduced.

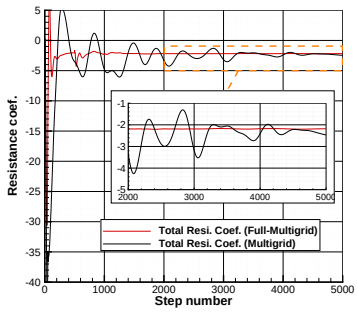

Figure 12: Convergence history of total resistance coefficient

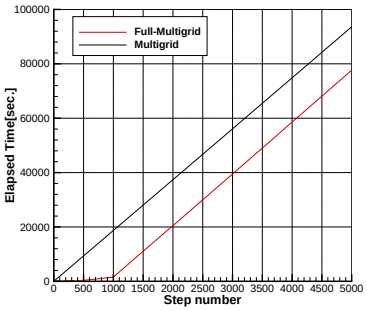

Figure 13: Comparison of elapsed time

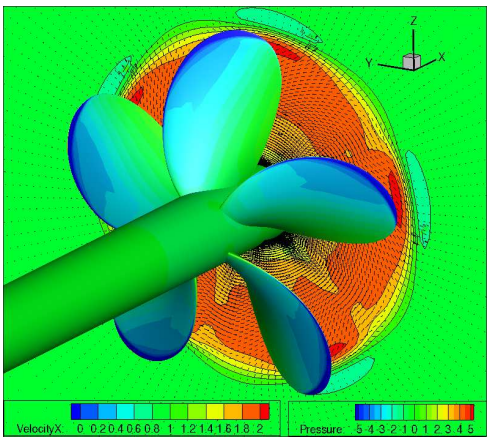

Figure 14: Pressure distribution on body surfaces and flow behind the blades

REFERENCES

[1] K., Ohashi, T., Hino, N., Hirata, H., Kobayashi, Development of NS solver with a structured overset grid method *The 28th Computational Fluid Dynamics Symposium*, Japan, 2014.

[2] H., Kobayashi, Y., Kodama, Developing spline based overset grid assembling approach and application to unsteady flow around a moving body, *MARINE2015*, Roma, Italy, June 15-17, 2015.

[3] C.L., Rumsey, T.B., Gatski, Recent Turbulence Advances Applied to Multielement Airfoil Computations, *Journal of Aircraft*, vol.38(5), pp.904-910, 2001.

[4] F.R., Menter, Two-Equation Eddy-Viscosity Turbulence Models for Engineering Applications, *AIAA Journal*, vol.32(8), pp.1598-1605, 1994.